Emission enhancement behaviors in the coupling between surface plasmon polariton on a one-dimensional metallic grating and a light emitter

Jyh-Yang Wang, Yean-Woei Kiang, and C. C. Yang[a)]
Institute of Photonics and Optoelectronics, Graduate Institute of Communication Engineering, and Department of Electrical Engineering, National Taiwan University, 1 Roosevelt Road, Section 4, Taipei, Taiwan 10617, Republic of China

(Received 10 October 2007; accepted 15 November 2007; published online 5 December 2007)

The authors study numerically the enhancements of dipole radiation rate and emission efficiency in a structure of a sinusoidal interface between a half space of metal and a half space of dielectric. The surface plasmon polaritons (SPPs) generated at the interface couple with the dipole to enhance its radiation rate. The energy dependence of radiation rate relies on the factors of SPP density of state, dipole position, and the emission efficiency. Below the light line, the emission efficiency is controlled by the localized surface plasmon (SP) field distribution in coupling two counterpropagating SPP modes near the Brillouin zone boundary. A localized SP field distribution of higher intensity and higher emission efficiency leads to a higher dipole radiation rate and a higher emission fraction. © *2007 American Institute of Physics*. [DOI: 10.1063/1.2821829]

When a light emitter is placed close to a metal structure on which surface plasmons (SPs) are generated, the coupling, through the interaction of the SP evanescent field with the light emitter, can enhance the emission efficiency.[1,2] The emission efficiency is enhanced via an alternative radiation channel, in which the energy of the light emitter is first transferred into the propagating or localized SP modes and then into the radiation modes. Such a coupling process for emission enhancement has been widely observed for semiconductor and organic light emitters.[3–8] The feasible emission enhancement factor of a semiconductor quantum well through the coupling with SPs has also been theoretically discussed.[9,10] However, the coupling behaviors, such as the energy dependencies of enhanced radiation rate and emission efficiency have not been well studied yet. In particular, with a metal grating structure, the coupling between the propagating and radiation SP modes becomes more effective. The coupling behaviors of SPs on a metal grating structure with a nearby light emitter need to be understood.

In this letter, we report the numerical study results on the coupling behaviors of a light emitter (a radiating dipole) with SPs generated at the sinusoidal interface between a half space of dielectric and a half space of Ag. For simulation, we use the boundary integral-equation method for the designated two-dimensional (2D) problem.[11] In this method, the unknown equivalent surface currents on the interface between the metal and dielectric are expanded with the local linear bases. The boundary integral equation is then transformed into a matrix equation for numerical computation. The geometry of the 2D problem is shown in the inset of Fig. 1. It consists of a one-dimensional sinusoidal boundary between the lower half space of dielectric material (refractive index at 2.5) and the upper half space of Ag. For numerical calculations, the period of the grating is set at 100 nm and the sinusoidal amplitude is 10 nm. An x-polarized dipole is placed near the grating structure in the dielectric 20 nm away from the dc line of the grating, i.e., at $y=-20$ nm. For comparison, we consider two dipole positions in the x axis with the one located right below a sinusoidal minimum (maximum) being denoted as p1 (p2). The Drude model of dielectric constant for bulk Ag is used[12] with the plasma frequency shifted to a value leading to the experimental resonance energy of surface plasmon polariton (SPP) at a flat Ag/GaN interface at 2.8 eV (denoted as ε_r).[13]

Figure 1 shows the enhancement factors of radiation rate as functions of energy for the cases of flat boundary and the grating structure with two dipole positions. The radiation rate of the dipole was obtained by integrating the outflowing power from a square boundary centered at the dipole location with 5 nm on each side. It represents the total power leaving the dipole, including direct radiation and that coupled into SPs. The enhancement factor of radiation rate is defined as the ratio of the radiation rate under a set of grating and dipole conditions to that in a structure of the lower half space of dielectric with a flat boundary covered by free space. In the case of flat boundary, the radiation rate increases from the low-energy side to reach a maximum at 2.72 eV and then decreases steeply on the high-energy side. On the low-energy

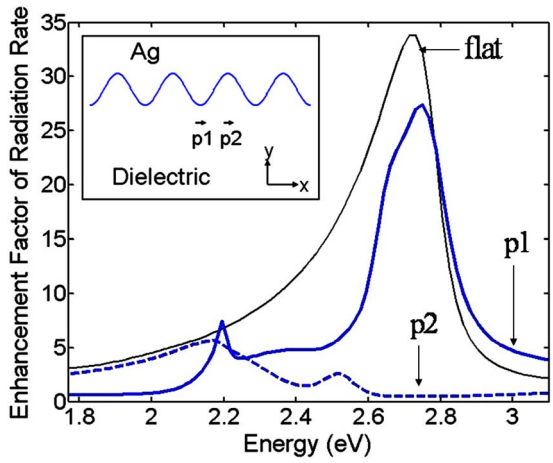

FIG. 1. (Color online) Enhancement factors of radiation rate as functions of energy for the cases of flat Ag/dielectric interface (labeled with "flat") and the grating structure with two dipole positions at p1 and p2.

[a)]Tel.: 886-2-23657624. FAX: 886-2-23652637. Electronic mail: ccy@cc.ee.ntu.edu.tw.

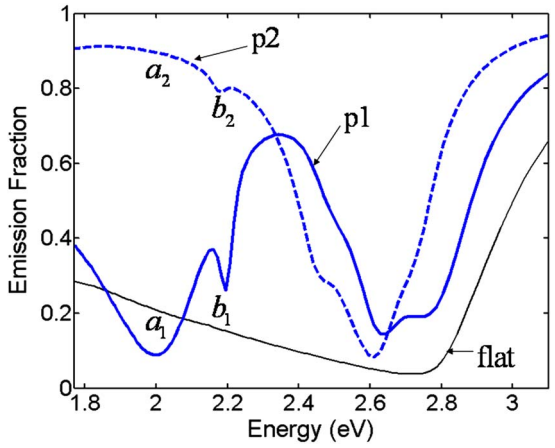

FIG. 2. (Color online) Emission fractions as functions of energy for the three cases in Fig. 1.

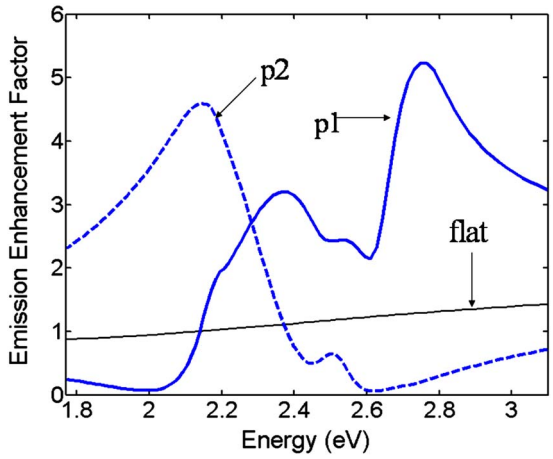

FIG. 3. (Color online) Emission enhancement factors as functions of energy for the three cases in Fig. 1.

side, the SPP density of state increases as energy approaches ε_r. With the dipole at p1, the enhancement factor of radiation rate shows the similar general energy dependence to the case of flat boundary except the minor peaks on the low-energy side. The enhancement factor approaches to unity at the low-energy end. However, by moving the dipole to p2, the major peak near ε_r disappears. Only a few minor peaks exist on the low-energy side with the enhancement factor approaching a level around 3 at the low-energy end.

Figure 2 shows the emission fractions as functions of energy for the three cases in Fig. 1. The emission fraction was obtained by evaluating the total power propagating downward across a horizontal boundary at 40 nm away from the dc line of the metal/dielectric interface. This total power was then normalized by the total radiated power as calculated for Fig. 1. Because there is no upward propagating power, an emission fraction in Fig. 2 represents the total emitted power. The difference between the emission fraction and unity is attributed to the loss. In the case of flat boundary, the emission fraction shows a slowly decreasing trend from the low-energy end to reach a minimum near ε_r and then increases steeply at the high energy end. The low emission fraction on the low-energy side is attributed to the momentum mismatches between the SPP modes and the radiation modes. The SPP loss reaches the maximum near the resonance energy such that the emission fraction has a minimum there. With the grating structure, the emission fractions also show minima near ε_r. However, on the low-energy side, the emission fraction behaviors are quite different. With the dipole at p2, the emission fraction shows a generally increasing trend with decreasing energy, in which a few minor dips can be observed. On the other hand, with the dipole at p1, in decreasing energy the emission fraction increases first and then shows a broad dip. A few minor dips are observed. The minima near ε_r are due to the high SPP loss.

In the SPP-dipole coupling process, a stronger SPP mode field or a higher SPP density of state leads to more effective energy transfer. In the case of flat boundary, near ε_r, the high SPP density of state results in strong SPP-dipole coupling and hence high radiation rate. However, the high SPP loss in this energy range leads to low emission fraction. In the cases of grating structure, one of the prominent features is that the dips in Fig. 2 around 2.2 eV (labeled as "b_1" with the dipole at p1 and as "b_2" with the dipole at p2) correspond to the peaks in Fig. 1 at the same energies. Those dips and peaks are attributed to the grazing-angle radiation of SPP along the x and $-x$ axes. This part of SPP radiation cannot be collected from the bottom side of the grating and, hence, leads to a reduction of emission fraction. However, with this part of field at the metal/dielectric interface, the enhanced SPP-dipole coupling increases the radiation rate.

Figure 3 shows the emission enhancement factors as functions of energy, which were obtained by multiplying the results in Fig. 1 with those in Fig. 2. Here, for the case of flat boundary, one can see the slowly increasing trend of emission enhancement with energy. The insignificant emission enhancement in this case is attributed to the fact that most of the dipole energy is coupled into SPP modes and dissipated by the metal. With the grating structure, when the dipole is at p1, two major peaks can be observed. The high (low) energy peak mainly originates from the high radiation rate (high emission fraction). With the dipole at p2, the emission enhancement factor shows a significantly redshifted broad major peak.

To further interpret the results in Fig. 2, we used the plane-wave-assisted boundary-integral equation method[11] to evaluate the dispersion relation of the SPP mode in the grating structure (see Fig. 4). In Fig. 4, the range of the in-plane wavevector k_x is between the center (k_x=0) and the boundary (k_x=31.4 μm^{-1}) of the first Brillouin zone. The line confining the gray region corresponds to the light line in the dielec-

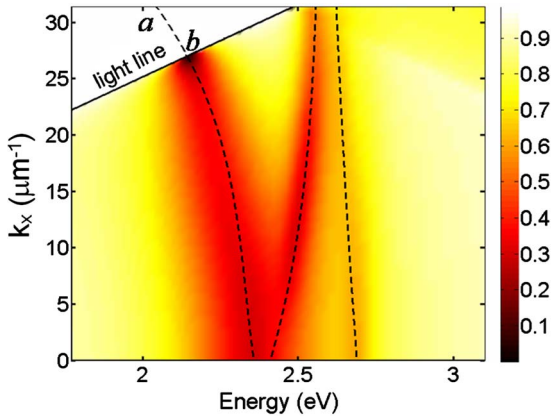

FIG. 4. (Color online) Dispersion relation of the SPP mode in the grating structure. The gray level represents the reflectance of the incident plane wave from the grating structure in numerical calculation.

tric, beyond which the dispersion relation cannot be plotted based on the used numerical method. In Fig. 4, we mark the dispersion curves based on the third-order polynomial fitting of the darkest locations (the minimum reflectance of the incident plane wave from the grating structure in numerical calculation). By extrapolating the dispersion curve of the lowest-energy section to reach the region beyond the light line and intercept the zone boundary, we can observe the interception point around 2.04 eV, which is designated as "*a*." The interception point of this dispersion curve with the light line around 2.14 eV (close to 2.2 eV) is designated as "*b*." The dip features at b_1 and b_2 in Fig. 2 correspond to the interception at *b*. At this point, the grazing-angle radiation of SPP leads to a dip in emission fraction and a peak in radiation rate, as discussed earlier.

In Fig. 2, the difference in the low-energy behavior labeled with "a_1" and "a_2" between the cases of two dipole locations deserves detailed discussion. As shown in Fig. 4, they correspond to the interception point at *a*. Near this energy, two counterpropagating SPP modes are effectively coupled with each other through the grating structure. Because the individual SPP modes are below the light line, they cannot radiate. However, the combination of the two mutually coherent SPP modes can form a localized SP field distribution that can couple into the downward radiation. Nevertheless, its emission fraction depends on the localized SP field distribution, which also controls the dipole radiation rate. Figures 5(a) and 5(b) show the E_x distributions of the localized SP field at 2 eV for the dipole positions p1 and p2, respectively. In either Fig. 5(a) or 5(b), the upper portion shows the line-scan profile of E_x at $y=-15$ nm. One can see that the amplitude of E_x is generally stronger in the p2 case. The line integral (along the *x* axis) of the upper portion is equivalent to the overlap integral of the SP field with a downward-propagating plane wave. This integral can be used to estimate the coupling efficiency of the localized SP field into the radiation in the direction of $k_x=0$. The line integral ratio of the p2 case over the p1 case is around 6.9, indicating that the radiation efficiency of the localized SP field in the case of p2 is much higher than that of p1. This result explains the difference between the features of a_1 and a_2 in Fig. 2. Also, with the stronger localized SP field in the case of p2 around 2 eV, the corresponding radiation rate is higher.

This research was supported by National Science Council Taiwan, Republic of China, under the Grant Nos. NSC 96-2120-M-002-008 and NSC-96-2221-E-002-188, and by US Air Force Scientific Research Office under the Contract No. AOARD-07-4010.

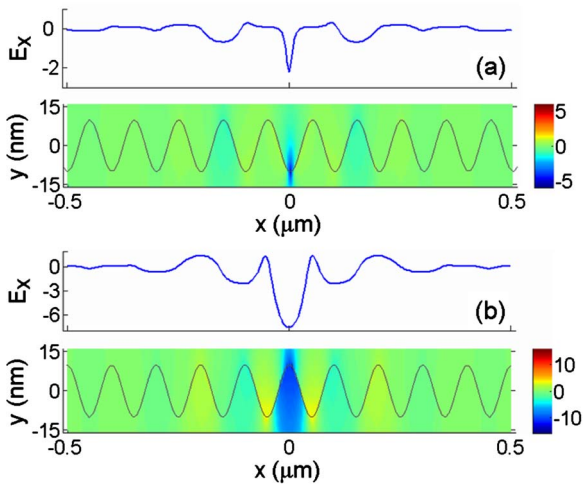

FIG. 5. (Color online) E_x distributions at 2 eV in the grating structure when the dipole is at (a) p1 and (b) p2. The upper portion of either part shows the line-scan field distribution at $y=-15$ nm.

[1] I. Gontijo, M. Boroditsky, E. Yablonovitch, S. Keller, U. K. Mishra, and S. P. DenBaars, Phys. Rev. B **60**, 11564 (1999).
[2] A. Neogi, C. W. Lee, H. O. Everitt, T. Kuroda, A. Tackeuchi, and E. Yablonovitch, Phys. Rev. B **66**, 153305 (2002).
[3] K. Okamoto, I. Niki, A. Shvartser, Y. Narukawa, T. Mukai, and A. Scherer, Nat. Mater. **3**, 601 (2004).
[4] C. Y. Chen, D. M. Yen, Y. C. Lu, and C. C. Yang, Appl. Phys. Lett. **89**, 203113 (2006).
[5] C. Y. Chen, Y. C. Lu, D. M. Yeh, and C. C. Yang, Appl. Phys. Lett. **90**, 183114 (2007).
[6] Y. C. Lu, C. Y. Chen, D. M. Yeh, C. F. Huang, T. Y. Tang, J. J. Huang, and C. C. Yang, Appl. Phys. Lett. **90**, 193103 (2007).
[7] D. M. Yeh, C. F. Huang, Y. C. Lu, C. Y. Chen, T. Y. Tang, J. J. Huang, K. C. Shen, Y. J. Yang, and C. C. Yang, Appl. Phys. Lett. **91**, 063121 (2007).
[8] S. Wedge, J. A. E. Wasey, W. L. Barnes, and I. Sage, Appl. Phys. Lett. **85**, 182 (2004).
[9] G. Sun, J. B. Khurgin, and R. A. Soref, Appl. Phys. Lett. **90**, 111107 (2007).
[10] J. B. Khurgin, G. Sun, and R. A. Soref, J. Opt. Soc. Am. B **24**, 1968 (2007).
[11] J. Y. Wang, C. C. Yang, and Y. W. Kiang, Opt. Express **15**, 9048 (2007).
[12] F. Wooten, *Optical Properties of Solids* (Academic, New York, 1972), pp. 52–55.
[13] K. Okamoto, I. Niki, A. Scherer, Y. Narukawa, T. Mukai, and Y. Kawakami, Appl. Phys. Lett. **87**, 071102 (2005).